Structural Surprises in Friction-Deposited Films of Poly(tetrafluoroethylene)

Dag Werner Breiby,*,† Theis Ivan Sølling,† Oliver Bunk,‡,§ René Bøgelund Nyberg,† Kion Norrman,† and Martin Meedom Nielsen†

Danish Polymer Centre, Risø National Laboratory, P.O. Box 49, 4000 Roskilde, Denmark, and Materials Research Department, Risø National Laboratory, P.O. Box 49, 4000 Roskilde, Denmark

Received April 19, 2004; Revised Manuscript Received December 7, 2004

ABSTRACT: Thin films of poly(tetrafluoroethylene) (PTFE) produced by friction deposition were studied using grazing incidence X-ray diffraction as the principal tool. The structure of the deposited thin films was compared with that of the surface of the PTFE bar used for depositing the films. Both exhibited the 15/7 helix conformation characteristic of crystal PTFE phase IV. A high degree of biaxial orientation was found for the highly crystalline thin films. Whereas the unit cell of the bar surface material appeared to be single-stem hexagonal, the film displayed diffraction characteristics consistent with a larger multistem unit cell. The origin of this increase of the unit cell is attributed to a higher degree of regular packing, possibly related to alternating right- and left-handed PTFE helices—a structure which has never been verified experimentally for PTFE in the 15/7 configuration. We discuss the possibility of a continuous transition between the low-order single-stem hexagonal and the multistem high-order unit cell. The degree of chain orientation was much lower at the surface of the bar than in the thin film. A modification of the commonly accepted mechanism for the transfer of material from the bar to the substrate is proposed.

Introduction

Poly(tetrafluoroethylene) (PTFE) is among the most important commercial polymers for highly demanding applications. Its areas of use range from structural parts to low-friction bearings and nonstick frying pan coatings. The versatility of PTFE is due to its unique physical and chemical properties, the best known being high hydrophobicity, very low friction coefficient, its thermal stability, and chemical inertness.

Partly because of its industrial importance, PTFE has received much attention also from the scientific community. It is now firmly established that bulk PTFE is highly crystalline, with helical chain molecules packed in essentially hexagonal arrangements, as first reported by Bunn and Howells.[1] Also, it has been known since the early work by Pooley and Tabor that the sliding of a bar of PTFE under pressure across a glass substrate leaves a thin, highly oriented film on the substrate.[2] These authors concluded from measurements of the (lateral) sliding force that also the PTFE crystallites near the surface of the bar itself became aligned in the process, as the friction coefficient decreased after repeated depositions. Following Wittmann and Smith's discovery that such friction-deposited, ultrathin PTFE films have the ability to induce oriented growth of a wide range of different organic molecules, liquid crystals, synthetic and natural polymers, and certain inorganic species and metals, scientific interest in these films and their use as orientation layers has surged.[3−5] Control of molecular orientation is a prerequisite to fully exploit the highly anisotropic optical and electronic properties of the functional molecules used within nanotechnology and molecular electronics. A detailed understanding of the friction deposition technique and appropriate characterization methods are needed to optimize the performance of the PTFE films.

In this article, we address structural aspects of ultrathin PTFE films, including their rich variety of crystal phases and phase transitions, which continues to hold surprise despite the relatively simple molecular structure of PTFE. The friction deposition mechanism is given particular attention. Several techniques have been employed in the characterization of the films, the most important being grazing incidence X-ray diffraction and time-of-flight secondary ion mass spectrometry (TOF-SIMS). Our conclusions at certain fine points appear to contradict, but also extend and unify, earlier reports. The findings are thought to be relevant both in an improved understanding of the solid-state behavior of PTFE and for the use of friction deposited films of this polymer as aligning substrates.

PTFE Structure

For reference purposes, we provide a brief summary presenting the various phases and crystal structures of PTFE. A characteristic of PTFE is that the individual $-[CF_2-CF_2]_n-$ chain molecules under conventional conditions adopt a helical shape, rather than a polyethylene-like zigzag arrangement, due to steric effects between the fluorine atoms.[1]

Bulk PTFE has several crystalline phases that apparently still are not completely resolved, as can be judged from the several somewhat different crystal unit cells proposed in the literature.[6] Generally, it is found that the almost cylinder-shaped molecules form crystals having a (pseudo-) hexagonal cross section. Previous PTFE structural studies using X-ray and electron diffraction have usually been conducted with bulk PTFE or drawn fibers,[1,7−9] but diffraction work is also reported for the thin friction-deposited films of concern in this article.[10,11] Atomic Force Microscopy (AFM) has been the preferred tool for many of the previous studies of these thin films.[12−14]

† Danish Polymer Centre.
‡ Materials Research Department.
§ Present address: Paul Scherrer Institut, Swiss Light Source, 5232 Villigen PSI, Switzerland.
* Corresponding author. E-mail: dag.werner.breiby@risoe.dk.

10.1021/ma0492465 CCC: $30.25
Published on Web 02/24/2005

At least four phases are known for bulk PTFE.[9] At ambient pressure, phase II exists below 19 °C,[8] phase IV is between 19 and 30 °C, and phase I is found above 30 °C.[9] In addition, a high-pressure phase III exists,[15] and there are also some reports of a high-temperature phase ($T > 150$ °C).[16] According to Clark and Muus, the hexagonal unit cell of phase IV is characterized by $a = b = 5.66$ Å, $c = 19.5$ Å, and the (pseudo-) hexagonal phase II by $a = b = 5.59$ Å, $c = 16.9$ Å, $\gamma = 119.3°$.[7] Throughout this article, the indexing is done using this bulk PTFE phase IV unit cell. An important characteristic of the phases is the degree of twisting of the macromolecules, which can be parametrized as a ratio u/t, where t is the number of turns per u repeat units. This is related to the pitch P and the interatomic spacing s along the (discontinuous) helix as $u/t = P/s$.[17,18] For the lower temperature phases the helices are more tightly twisted. Molecular resolution images of the helical chains are reported both using transmission electron microscopy (TEM)[19] and AFM.[12]

In phase II, below 19 °C, the helices form a "pseudo-hexagonal" (triclinic) packing of alternating left- and right-handed helices having a u/t value of approximately 13/6. A large degree of hysteresis is associated with the first-order phase transition at 19 °C.[9] In phase III the helical structure of the macromolecules is lost due to the high pressure; the helix is apparently completely untwisted changing the molecular conformation to a zigzag.[15] The 1.3 Å C−C repeat distance along the backbone is virtually independent of the phase. This periodicity results in the 0013 and 0015 reflections for 13/6 (phase II) and 15/7 (phase IV), respectively (see below).

Arguably, the most important bulk phase is the intermediate "phase IV", existing at 1 atm pressure for 19 °C < T < 30 °C. It appears to be general agreement that this phase has 15/7 helices packed in a single-stem hexagonal unit cell,[6] however, with the notable exception of Farmer and Eby,[20] who propose a pseudohexagonal cell with *four* molecular stems based on energy calculations. From these theoretical studies, it was concluded that the energetically optimal packing of PTFE molecules is with every second molecule having the opposite handedness. It was further predicted that like-handed molecules lie closer by about 0.2 Å compared to what is the case for an even-handed pair. Rather elaborate considerations were given on the setting angles (about the molecular axes) between adjacent molecules.[20] However, moving entire chains or, alternatively, retwisting chains from one handedness to the other is an obviously energy consumptive and unlikely event. Monte Carlo simulations, conducted for the 19 °C phase transition,[21] suggest that the chains can order in crystalline domains of every other molecule being right- or left-handed by having *both* right- and left-handed segments in individual chains, separated by mobile, soliton-like defects.[20,22−24]

Structure As Seen by Diffraction. Following the standard formalism of diffraction,[25] the unit cell and its orientation determines the peak position for a given (hkl) lattice plane by Bragg's law, and the intensity of each reflection is proportional to the square of the structure factor, $|F|^2$. The most striking effect of the helix structure factor is the resulting "layer lines (strictly, planes) l" in reciprocal space. These layers are equidistantly spaced and perpendicular to the chain axis.[17] The radial distribution of scattered intensity $f^l(r)$ within each plane can be modeled by a sum of Bessel functions $J_n(r)$. It can be shown that for a u/t helix the following selection rule must be obeyed[9,17]

$$l = tn + um \tag{1}$$

where l denotes the lth layer line, n is the order of the Bessel function, and m is an arbitrary integer. As the Bessel functions vary slowly as a function of r, they can be considered envelope functions modulating the intensity of the sharp (Bragg) peaks from the crystal lattice.

According to (1), for a $u/t = 15/7$ helix one expects zeroth-order Bessel functions for the layers {0, 15}, first order for {7, 8}, and second order for {1, 6, 9, 14}. $J_0(r)$ has a strong maximum at $r = 0$ (on the meridional axis); the higher order Bessel functions $J_n(r)$ have their first maximum at radii increasing monotonically with order n. Note that whereas the meridional reflection at the reciprocal point $c^* \sim 2\pi/1.3$ Å^{-1} corresponds to the 0013 reflection for the 13/6 phase, it is the 0015 reflection for 15/7. Some issues related to diffraction from hexagonally packed helices are summarized in Figure 1.

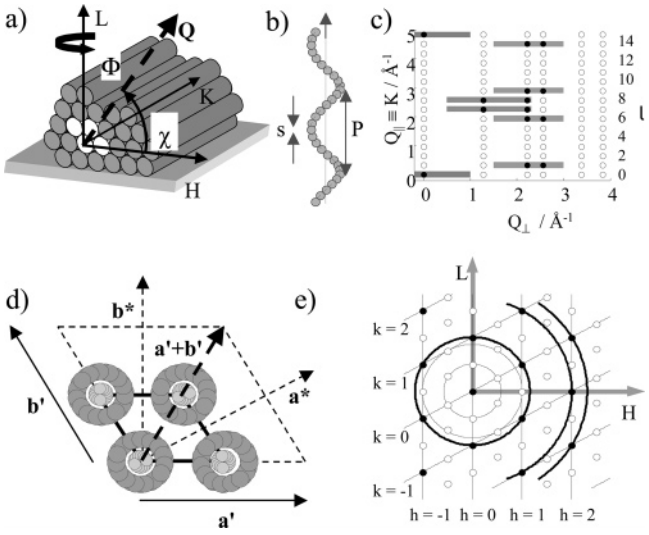

Figure 1. Illustration of the diffraction resulting from a crystal of hexagonally packed helices. (a) Hexagonally packed PTFE chains. (b) A discrete helix with 15 units per turn (i.e., a 15/1 helix). P denotes the pitch of the molecule, and s is the projection of the intrachain spacing onto the molecules' center axis. (c) The expected diffraction pattern for a 15/7 helix, assuming cylindrical symmetry about the fiber axis, with $Q_\perp = \sqrt{(H^2 + L^2)}$. (d) Both a single-stem and a four-stem unit cell with $a' = 2a$, $b' = 2b$ are indicated. **a*** and **b*** denote the reciprocal lattice vectors. **c*** is parallel to **c**, which is directed out of the paper plane. (e) A map of the reciprocal lattice corresponding to the structures in (d). Filled circles are reflections consistent with a single-stem unit cell. Open circles are additional potential reflections in the case of a four-stem unit cell. The circle segments (constant Q) serve as guides to the eye.

The dimensions indicated in Figure 1 are approximately those expected for the bulk PTFE phase IV. The strong Bragg peaks (filled circles, Figure 1c) represent maxima in the convolution of the scattering from the hexagonal unit cell (circles) by the structure factor of the 15/7 helix, giving layers l with a $Q_\perp$ (radial) intensity distribution governed by Bessel functions J_n. Higher order n gives weaker maxima at larger radii, as illustrated by the shaded patches for n up to second order.

Experimental Section

Preparation of the PTFE Films. The PTFE used in our studies was standard, sintered bulk Teflon. The purity of the

PTFE was confirmed using X-ray photoelectron spectroscopy (XPS). A rectangular bar of lateral dimensions 10 × 23 mm^2 and thickness ∼10 mm was cut. The sliding was performed along the short dimension of the bar and always in the same direction. Microscopy glass slides rinsed in 2-propanol for about 15 min and then flushed dry using argon were used as substrates. Just before depositing the PTFE, the substrates were wiped off with ethanol using a clean-room napkin in order to remove the last few visible grains of dust from the surface. Substrates with the slightest visible defects were rejected.

The friction deposition was made using a motorized apparatus enabling control of the sliding rate, pressure, and temperature.[10] Both the stage holding the glass slide and the brass holder for the PTFE were heated in order to minimize the temperature gradients across the system. The deposition temperatures were in the range from 150 to 320 °C, the latter being close to the PTFE melting point of ∼330 °C. The applied loads were 5 and 10 kg, corresponding to about 0.2 and 0.4 MPa pressure. The sliding rate was varied between 0.9 and 4 mm/s. It proved important for the quality of the films that the PTFE bar was tightly fastened, i.e., that the setup did not allow any sideways or rotational movements of the bar.

An important preparation for the film fabrication was to make a considerable number (∼100) of "alignment depositions", most of these at a high temperature ∼300−320 °C in order to have a significant material transfer. These depositions had the purpose of leveling the surface of the PTFE bar and to simultaneously orient the polymer on the surface of the bar as described in the literature.[2] At the time of the diffraction experiments, the samples had been kept in a sealed container for about 3 days after deposition.

X-ray Diffraction. Grazing incidence X-ray diffraction (GID)[25] was performed using the z-axis diffractometer at the wiggler beamline BW2 at the Hamburger Synchrotronstrahlungslabor (HASYLAB). The sample was mounted horizontally with an additional rotational freedom Φ about the sample normal.[26] The wavelength used was 1.2398 Å, corresponding to an energy of 10 keV. The incidence angle α_i was fixed at 0.16°. At grazing incidence angles lower than a critical angle α_c ∼0.18°, the beam is totally reflected from the substrate, effectively enhancing the signal from the thin film.[25]

The sample stage was placed in a cylindrical chamber with helium atmosphere to reduce air scattering. The chamber wall was made of Kapton foil, which is virtually transparent to X-rays. A Cyberstar scintillation point detector was used for recording the signal. The detector can be positioned on a semisphere, determined by the two angles $2\theta_z$ (in the plane of incidence) and $2\theta_{xy}$ (perpendicular to the plane of incidence), having their origin at the interception with the direct beam. The total scattering angle 2θ is given by $\cos 2\theta = \cos 2\theta_{xy} \cos 2\theta_z$. The scattering vector $\mathbf{Q}$ is defined by $\mathbf{Q} \equiv \mathbf{k_{out}} - \mathbf{k_{in}}$, where $\mathbf{k_{in}}$ and $\mathbf{k_{out}}$ denote the in- and outgoing wave vectors, respectively. Only elastic scattering is considered here; thus, $|\mathbf{k_{in}}| = |\mathbf{k_{out}}|$.

We employ an orthogonal reciprocal lattice H, K, L with units of Å^{-1}. The lattice is oriented with K directed in the PTFE chain direction, H is the other in-plane direction being perpendicular to the chains, and L is the out-of-plane direction (cf. Figure 1). The angle χ denotes the angle of $\mathbf{Q}$ with respect to the sample surface. Software routines enable H, K, and L to be changed (scanned) by changing sample and/or detector position.[26] As an example, to perform an H-scan with $K = L = 0$ corresponds to (stepwise) moving the detector ($2\theta_{xy}$, $2\theta_z$) and the sample (Φ) such that the length Q of the scattering vector is varied, while keeping $\mathbf{Q}||\mathbf{H}$. Also scans probing the orientational distribution function ("rocking scans") were performed. These scans are done with the detector in a fixed position ($2\theta_{xy}$, $2\theta_z$) corresponding to a designated Bragg peak (constant $\mathbf{Q}$). Rotating the sample about the L axis (angle Φ) effectively probes the in-plane alignment (cf. Figures 1 and 2). Similarly, rotations about K (angle χ) probe the orientation about the axis of the molecular chains. For any coordinates (H, K, L) with diffracted intensity, there is a corresponding real-space lattice spacing $d = 2\pi/Q = 2\pi/(H^2 + K^2 + L^2)^{1/2}$.

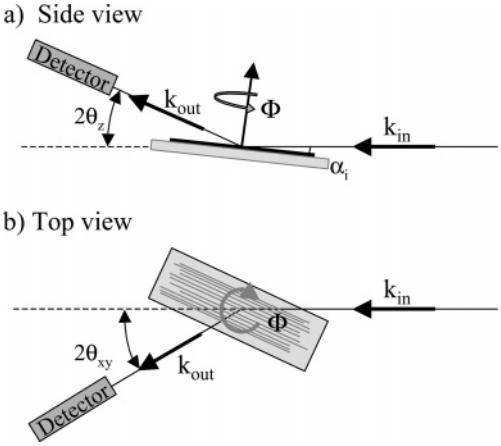

Figure 2. Geometry of the grazing incidence X-ray diffraction (GID) measurements. In (a) the sample is seen from the side and in (b) from above.

From the peak widths, information on the correlation length and the strain of the crystalline domains can be obtained. Neglecting residual stress in the material, the Scherrer formula[27] provides a simple parametrization in terms of a *crystallite dimension* parameter Γ

$$\Gamma = \kappa \frac{2\pi}{\Delta Q} \tag{2}$$

where ΔQ is the fwhm of the peak and $\kappa \approx 0.9$ is a constant depending on the scattering geometry.

Simulations. Using the coordinates for a helical PTFE 15/7 molecule as given in ref 20, structure factor calculations for PTFE crystal lattices were carried out. The molecules were treated as rigid objects, i.e., with no internal degrees of freedom. The structure factor F was calculated using the formula

$$F = \sum_j f_j \exp(2\pi i(hx_j + ky_j + lz_j)) \tag{3}$$

where f_j is the (scalar) atomic form factor and x_j, y_j, z_j are the (fractional) crystal coordinates of atom j. hkl denotes the Miller indices. The simulated peak intensities, being proportional to $|F|^2$, were corrected for preferred orientation using the experimental rocking curves for normalization. Lorentz and polarization corrections were applied as described in ref 28.

An important observation from (3) is that F is independent of z for equatorial reflections ($l = 0$). In other words, the observed structure is then the projection of the helices into rings in the $a-b$ plane, which implies that along-chain features like handedness and setting angles are not resolved. On the other hand, the simulations verified that the equatorial diffraction patterns are very sensitive to small displacements δ of the $a-b$ position of the molecules. A consequence is that for, say, a two-stem cell there are only two adjustable parameters describing the (relative) displacement of one stem with respect to the other. Similarly, for a four-stem cell, there are $3 \times 2 = 6$ parameters influencing the equatorial reflections.

TOF-SIMS. Time-of-flight secondary ion mass spectrometry (TOF-SIMS)[29] analyses were performed using a TOF-SIMS IV (ION-TOF GmbH, Münster, Germany). High lateral resolution images (∼200 nm) were obtained using 160 ns pulses of 25 keV Ga^+ at a repetition rate of 10 kHz, thus yielding a target current of 0.5 pA. These primary ion conditions were used to scan 50 × 50 and 10 × 10 μm^2 areas of the samples. An electron gun was used to minimize charging of the surface. Desorbed secondary ions were accelerated to 2 keV, mass analyzed, and post-accelerated to 10 keV before detection. TOF-SIMS imaging provides information about the lateral distribution of surface chemistry.

Results

Morphology. TOF-SIMS imaging[29] probes very large areas (up to cm^2) compared to AFM. In agreement with

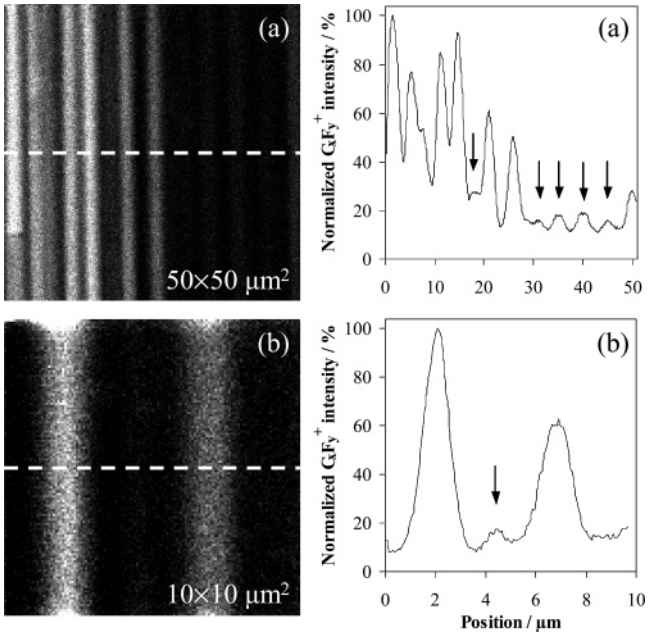

Figure 3. TOF-SIMS ion images (left pictures) constructed from the sum of $C_xF_y^+$ intensities obtained from an optimal, friction-deposited film. The graphs to the right are intensity profiles across the ion images (dashed lines). The TOF-SIMS technique shows that the PTFE material is oriented over regions of many micrometers or even millimeters. The arrows indicate smaller fiber bundles.

previous results, we found that the friction-deposited PTFE thin films consist of very long (several hundred microns) and straight bundles of ribbons lying flat on the substrate.[3,10,14] The thickness of the PTFE films varies between 15 and 80 nm and the coverage between ~30 and ~95%. Corroborating earlier work,[3,10,14] these values depend strongly on the three main deposition parameters: sliding rate, temperature, and pressure. Optimization of these values was attempted during repeated deposition series and yielded information regarding the optimal temperature T_{opt} for a homogeneous film formation.

The optimized values for the sliding rate and load pressure were found to be 0.9 mm/s and 10 kg, respectively. For the first film depositions, the optimal temperature T_{opt} was approximately 310 °C, but during the subsequent 30−40 depositions T_{opt} decreased to about 250 °C. Unexpectedly, when restarting to deposit films 3 weeks later using the same PTFE bar, friction deposition at 250 °C yielded poor films, as evaluated using AFM (not shown). The ribbons were not fully parallel to the sliding direction, and the coverage was low. The optimal temperature was again found to be 310 °C, suggesting that relaxation had taken place in the bar in the 3 week interval.

From the TOF-SIMS images, we estimated the coverage of the best PTFE films to be 90−95%. Figure 3 shows TOF-SIMS images of the long and straight PTFE ribbons. The lateral resolution (~200 nm) of TOF-SIMS is insufficient to visualize the individual ribbons and grooves that have been observed using e.g. AFM,[14] but this technique demonstrates that there is a high degree of alignment of the PTFE material.

Grazing Incidence X-ray Diffraction. GID studies were performed on selected, high-quality PTFE films and on the PTFE bar; the latter was studied to gain more information about the deposition mechanism. Figure 4 shows the data resulting from a Φ scan

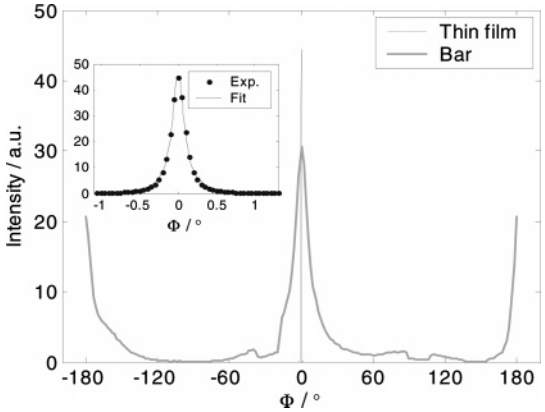

Figure 4. Φ-rocking scans for the bar and for the thin film, with $Q = 4.83$ Å^{-1}, corresponding to the 1.3 Å C−C distance. The minima in the intensity for the data obtained for the bar at about −20 and 100° are due to shadows from the sample cell. The arbitrary axis zero was taken at the maximum intensity. The inset shows a magnified view of the extremely narrow distribution for the friction-deposited film, with the solid line being a fitted Lorentzian.

("rocking scan", $\mathbf{Q}$ = constant) for the 1.3 Å repetition distance in crystalline PTFE. This is the 0015 reflection for the PTFE bulk phase IV. In accordance with previous AFM studies,[14] the bar was found to have a rather high degree of orientation, with a distribution width $\Delta\Phi_{fwhm} \sim 15°$. However, this degree of alignment is actually poor compared to that observed for the films, which exhibited $\Delta\Phi_{fwhm}$ as low as 0.23°. This width was remeasured several times with narrow slits (good instrumental resolution), ensuring that the measured width approaches the true width of the distribution. This peak was very intense, despite its high Q value of 4.83 Å^{-1}.

For the thin film sample, the data presented in Figure 4 were collected over a short angular range. The geometry-dependent corrections for absorption and effective scattering volume can therefore be neglected as they only contribute with an essentially constant scaling factor.[30] For the bar, however, the long footprint of the beam (of the order of a centimeter) combined with the geometry of the bar might give a nonnegligible Φ dependence to the measured intensity. A worst-case estimate is that the peak-to-background intensity of the rocking scan should be rescaled by a factor ~2.7, being the ratio of the lateral dimensions of the bar. Clearly, this would not alter the perception that the degree of orientation in the bar was *much* lower than in the film. This observation has important consequences for the understanding of the transfer mechanism of PTFE from the bar to the substrate (cf. Discussion). A frequently used measure of uniaxial orientation is the Hermans (nematic order) parameter $S \equiv 0.5(3\langle\cos^2\Phi\rangle - 1)$, which ranges from 0 for isotropic materials to 1 for perfectly aligned materials. The data in Figure 4 yield the values $S > 0.99$ and $S \sim 0.8-0.9$ for the film and the bar, respectively.

Scans performed in the H direction (in-plane, equatorial) for both the film and the bar are shown in Figure 5. The highly ordered thin films displayed a pronounced peak of "$^1/_2{}^1/_2$0" type (same lattice spacing as 1−$^1/_2$0) at 1.11 Å^{-1} and a small hump "$^1/_2$00" at 0.64 Å^{-1}. Confer Figure 1e for a map of the reflections. Generally, the sharper peaks of the thin film as compared with the bar data imply longer ranging order. It can be seen from the figure that the width of the "1−$^1/_2$0" peak is

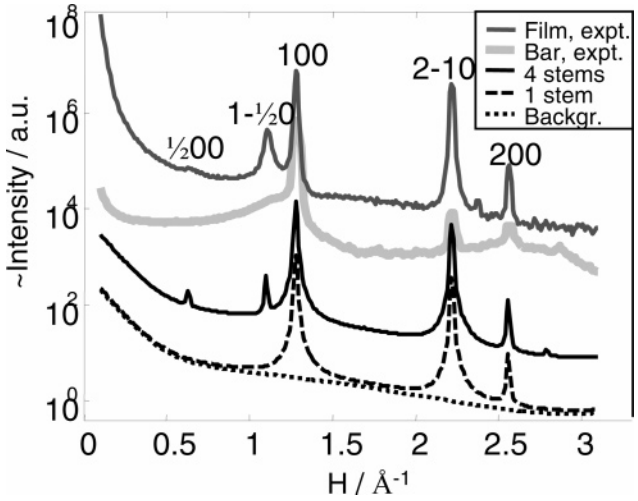

Figure 5. Experimental data and simulations of H scans (for $K = 0$, $L = 0.03$) are shown, with scaling factors chosen to increase readability. The peaks denoted 100 and 200 are tails of the strong $h00$-type reflections (the maxima of these peaks are at $\chi = \pm 30°$). Also, a 2−10 peak is observed in both film and bar. An important qualitative difference between the scans of the film and the bar is that two unexpected fractional index peaks appear for the film. For the bar, only the $1-{}^1/_20$ reflection partly remains, as a shoulder to the 100 peak. The peaks are significantly broader for the bar, indicating that the crystalline correlation length is shorter. Simulations are shown both for a single-stem cell, corresponding to the model of Clark et al., and for a unit cell with four stems. As expected, the single-stem model gives no crystalline signal below the 100 peak.

significantly broader than for the 100 peak. By fitting Gaussians to the peaks, we found a peak width of 0.023 ± 0.002 Å^{-1} for the $h00$ peaks, corresponding to a correlation length Γ of about 250 Å by (2). The width of the "$^1/_2{}^1/_20$" was about 0.044 Å^{-1}, suggesting Γ ∼130 Å and thus that this peak is of a different nature than the $h00$ peaks. For the bar, the peak-to-background ratio increased with higher incidence angles α_i, suggesting that the oriented crystallites protrude into the interior (bulk) of the bar.

Results of the structure factor simulations are also shown in Figure 5. As expected, no Bragg peaks are found below 100 for the single-stem unit cell of Clark et al. It was not possible to obtain a good fit for a double-stem model. The other presented simulation was done for a four-stem hexagonal unit cell, with $a = b = 2 \times 5.66$ Å = 11.32 Å, $c = 19.5$ Å. To obtain a nonzero structure factor for the "new" peaks, several small lateral shifts of the molecules with respect to each other were tried. For the fit presented in Figure 5, the molecules at positions 1 and 3 (starting at the lower left corner, counting counterclockwise, cf. Figure 1d) were slightly displaced toward each other. The displacement of both molecules 1 and 3 for the simulation in Figure 5 was $\delta = 1.2/100 \times |\mathbf{a} + \mathbf{b}| = 0.14$ Å. This simple model gives a reasonable fit, but we do not claim that it is a unique solution.

Keeping Q constant and rotating the $\mathbf{Q}$ vector about the K axis (angle χ), the "rotational orientational distribution function" (R-ODF) of the crystallites was probed. The results are shown in Figures 6 and 7. With the GID method, χ values larger than ∼80° cannot be obtained. These scans demonstrate that the PTFE crystals have a densely packed lattice plane parallel to the substrate, as reported earlier from electron diffraction by tilting the sample.[10] With the GID technique,

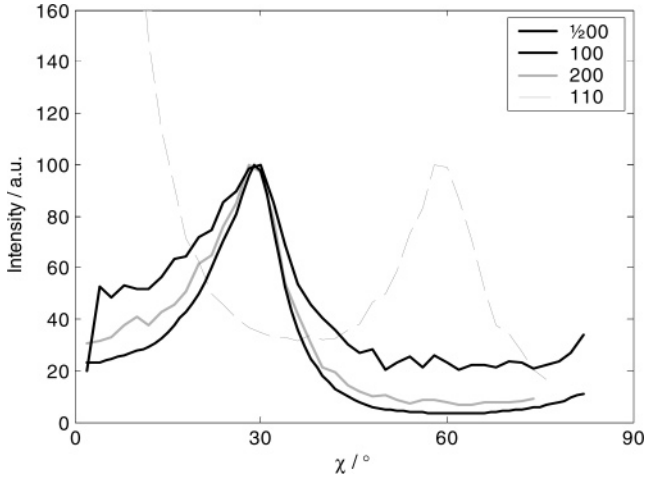

Figure 6. Rocking scans of χ showing that the $h00$ reflections are at 30° and 90°, whereas the 110-type reflections are at 0 and 60°. The $1-{}^1/_20$ peak is not shown because of problems separating it from the strong signal of the neighboring 100 peak, but it does indeed exhibit the same symmetry as the 110 peak. The intensities are rescaled for increased readability.

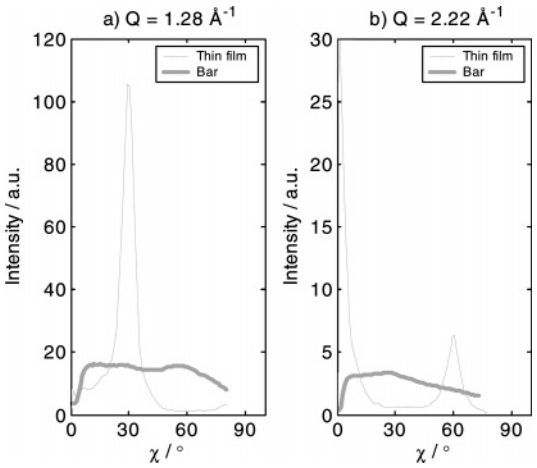

Figure 7. Comparison of the χ-rocking scans for (a) 100 and (b) 110 peaks obtained for the thin film and for the bar.

we can readily measure and quantify the width of the distribution, yielding $\Delta\chi_{fwhm} \sim 8 \pm 2°$. Thus, taken together with the Φ scans, it is clear that the crystallites in the film have a high degree of so-called "double" (biaxial) orientation.

Another observation from Figure 7 is that the R-ODF of the PTFE bar was almost isotropic (uniform in χ). However, upon closer inspection, it appears that there was a tendency for the crystallites in the bar of being rotated around the molecular axis by about 30° with respect to those in the film.

As described, the helical shape of the PTFE macromolecules gives rise to characteristic layer planes. The result of a K scan through the 100 peak ($H \sim 1.11$ Å^{-1}, $L \sim 0.63$ Å^{-1}, $\chi = \text{atan}(L/H) = 30°$) is shown in Figure 8, revealing that the 15/7 layer motif is indeed present (see also Figure 1c). It is readily seen that strong reflections are obtained for $l = \{0, 1, 6, 7, 8, (14),15\}$. Except for the low intensity of the $l = 9$ peak, the observed lines correspond to allowed low-order (zeroth, first, and second) Bessel functions by the selection rule (1). This is firm evidence that the room-temperature thin film has the helix 15/7 hexagonally packed phase.[9] This feature is well captured also in the simulations,

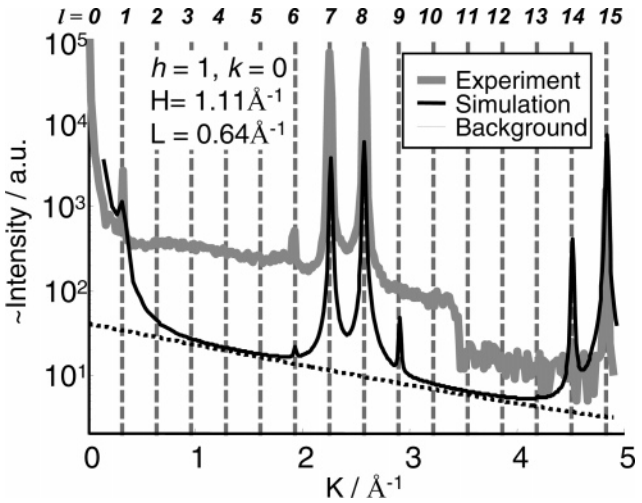

Figure 8. Experimental K scan (parallel to the molecular axis) performed on an high-quality thin PTFE film, starting in the 100 peak ($H = 1.11$ Å^{-1}, $L = 0.64$ Å^{-1}). A simulation is also shown, capturing the main features of the measured data. The interval from 0 to $2\pi/1.33$ Å $= 4.83$ Å^{-1} has been divided into 15, as indicated by the vertical broken lines. The effect of the helical structure factor is clearly seen, as indicated by the pronounced 100, 101, 106, 107, 108, 109, 1014, and 1015 peaks. The minimum in intensity for $K \in (3.3, 4.7)$ Å^{-1} is due to shadowing from the sample container.

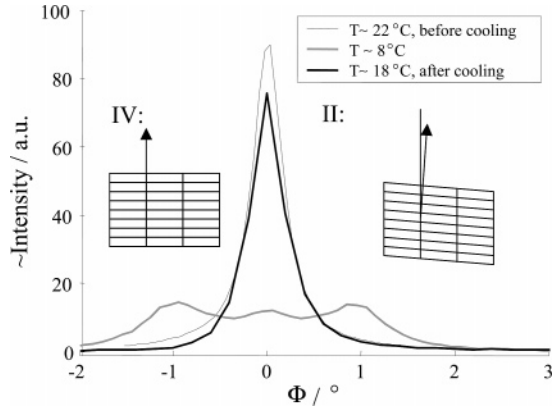

Figure 9. Temperature dependence of the 0015 peak. Note the splitting of the peak at the lowest temperature, interpreted as coexistence between two phases II (triclinic, low T) and IV. The arbitrary zero of the Φ rotation was taken at the maximum intensity.

albeit the structure factors are not in full agreement with the experimental data.

A preliminary attempt of measuring the low-temperature phase II is shown in Figure 9, displaying Φ "rocking" scans of the 1.3 Å peak before, during, and after cooling. Referring to Figures 2 and 4, we remind the reader that this kind of scans probes the alignment of the unit cells, yielding one sharp peak for the room-temperature phase. As it is known that a considerable hysteresis is associated with the 19 °C phase transition, we take the triple peak recorded at 8 °C to indicate the coexistence between the room-temperature phase (the center peak) and a low-temperature oblique phase. A doubling of the off-equatorial peaks has also been observed using TEM.[31] Figure 9 demonstrates the important fact that the thin PTFE films indeed exhibit a phase transition from a pseudohexagonal to a triclinic phase upon cooling. Evidently, also the low-T phase was highly oriented. When remeasuring at room temperature, a single peak was again measured, being somewhat broader and weaker than before visiting the low-T phase.

Discussion

PTFE Transfer and Film Formation. The optimal experimental parameters for friction deposition of a uniform PTFE thin film tend to vary from one report to another. In our study the best deposition conditions turned out to be temperatures just below the PTFE melting point, moderate pressures of about 0.4 MPa, and low speeds of about 0.9 mm/s. These conditions, being similar to those commonly described in the literature,[3,10,14,19] give thin transfer films that almost completely cover the substrate. Smooth continuous films with complete coverage could not be obtained; it appears that the highly corrugated surface is an intrinsic property of these films. As mentioned, we found that T_{opt} decreased substantially from about 300 to 250 °C after numerous depositions; however, reproducing these depositions of optimal thin film at 250 °C failed after the PTFE bar had been left unused for a period of 3 weeks.

The deposition temperature must be above 150 °C and below the melting point of $T_m \sim 330$ °C. Above 150 °C, PTFE softens, indicating that a phase transition takes place at this temperature, as is indeed reported.[16] If the temperature was too high (near the melting point), the deposited film was not well-aligned, as most of the material deposited by tearing. Bodö and Schott conjectured that the structure of the thin transfer film was formed during the cooling step following the deposition.[14] However, this would imply that it should be possible to modify the film structure by controlling the cooling conditions and possibly also by annealing the film. To the contrary, our experiments indicate that neither the cooling conditions nor annealing had any effect on the resulting film morphology.

The pressure applied to the PTFE bar during deposition also played an important role: Increasing the pressure increased the coverage and thickness until saturation at about 0.2−0.4 MPa. According to Bodö and Schott, there is actually a decrease in coverage when increasing the pressure above ~0.2 MPa.[14] The sliding rate had to be kept low, as the material transfer from the bar to the substrate was found to be reduced at increased sliding rate. As in the case of a too high temperature, a too low sliding rate resulted in material transfer by irregular release of "lumps" rather than the formation of a homogeneous film.

No influence of the thermal history of the PTFE bar on the resulting films was observed. Virgin, solid-state compacted PTFE (Teflon 6C, Du Pont) that has never been melted is therefore not entangled. To our surprise, the friction deposition of this material proceeded in a similar manner and resulted in similar films, as sintered, i.e., molten and recrystallized, fully entangled polymer. This observation is remarkable in view of the fact that virgin, entanglement-free PTFE can be deformed by tensile deformation to draw ratios well in excess of 100 (the very basis of the production PTFE membranes known as Gore-tex), whereas once-molten and solidified PTFE can be drawn only to a draw ratio of about 7. It is thus clear that friction deposition involves mechanisms that are fundamentally different from tensile deformation and is not affected by the number of entanglements per macromolecular chain. This issue is raised earlier in connection with friction-

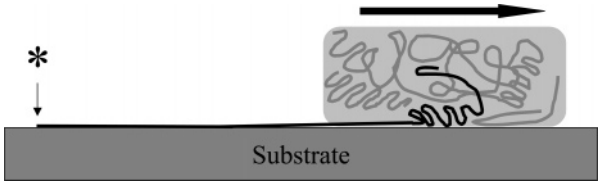

Figure 10. Illustration of the mechanism for friction deposition of PTFE onto a substrate. The asterisk indicates the initial anchoring point of the PTFE fiber, and the thick arrow gives the sliding direction of the bar.

deposition experiments with gel-processed, disentangled and melt-crystallized, fully entangled ultrahigh molecular weight polyethylene (UHMW PE).[4]

Pooley and Tabor advanced already in the early 1970s a deposition model for friction deposition of PTFE onto substrates; after repeated depositions, the PTFE strands get oriented within the bar and are subsequently transferred to the substrate.[2] The present data are consistent with a significant ordering of the PTFE bar, as reported also using AFM.[14] However, an important new aspect of the transfer mechanism is that, rather than entire crystallites being transferred, polymer strands, or even single chains, get attached to the substrate and are subsequently "pulled out" of the bulk and deposited under a tension, as illustrated in Figure 10. This mechanism accounts for both the completely straight and aligned polymer strands, the fact that the bar is less oriented than the film, and the observation that "disentangled" and "entangled" polymers behave in the same manner. This phenomenon is coined "chain pull-out" or "forced reptation"[32] due to its resemblance with de Gennes' concept of reptation (wormlike movements) in entangled polymers,[33] of course with external forces causing the polymer reptation in the present case.

Thin Film Structure. Previous studies of PTFE crystal structures have mainly been carried out on fibers of the polymer.[9] It appears that the structure of those fibers, having cylindrical (uniaxial) symmetry, resembles that of the structure of the PTFE *bar*, which exhibits only weak χ dependence. This is supported by the equatorial Bragg peaks shown in Figure 5, being in excellent agreement with the unit cell proposed by Clark et al.[7]

The thin films, by contrast, exhibit qualitatively different diffractograms. Notably, the crystallites in the film are highly biaxially oriented, i.e., not only in but also about the chain axis direction. The integral-order Bragg peaks were found at the same positions as in the bar, but they were also sharper, indicating an increase in correlation length by a factor ~2−3 (cf. eq 2).

The presence of fractional indexed peaks indicates that the single stem (pseudo-) hexagonal unit cell is too small. The presented fit for a four-stem cell having two molecules "attracted" to each other along the diagonal was the simplest model we found that gave a reasonably good fit to the data. As mentioned, it was also attempted with a double-stem orthogonal cell, but no appropriate fit was obtained.

We interpret the increase of the unit cell as being due to a regular packing of alternating right- and left-handed helices, as predicted by Farmer and Eby.[20] A sketch of some differently oriented crystalline domains is given in Figure 11, along with some possible unit cells. We stress that the peaks having Q values smaller than the 100 peak imply that the unit cell must be larger than the conventional single-stem cell in a hexagonal

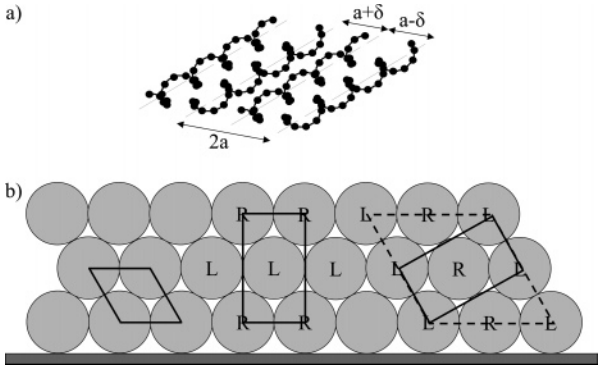

Figure 11. Sketch of crystalline packing in PTFE. (a) Example of a plane with alternating left- and right-handed helices, where a small shift $\delta \neq 0$ would increase the periodicity from a to $2a$. For simplicity, only single-stranded helices are drawn. (b) The equatorial cross section of a single-stem hexagonal, two double-stem orthorhombic, and a four-stem hexagonal unit cells are shown.

arrangement. The fit presented in Figure 5 is for a four-stem hexagonal unit cell, with two of the molecules slightly displaced to yield appropriate structure factors. Without the displacements of the molecules, the unit cell is effectively that of Clark et al. (the structure factor is then zero for fractional hkl), and it does not lend support to the observations. As $l = 0$ for the equatorial scans shown in Figure 5, this implies that the projection of the molecules must have a periodicity of $2a$ rather than a (cf. Figure 11a).

The observation that the $1-{}^1/_20$ peak is significantly broader than the other peaks indicates that the correlation length related to the lattice spacing $2a$ is shorter than for the other lattice planes. (For the ${}^1/_200$ peak the intensity was too low to obtain a reliable estimate of the width.) This supports a structure with long-range ordered hexagonally packed molecules, with (smaller) domains of periodically ordered handedness. Related to this issue is also the fact that we did not observe higher order fractional index peaks. We suggest that shorter-ranging order of the R−L−R−L−... pattern than of the hexagonal packing gives a quicker decreasing intensity with increasing Q for the fractional index peaks.

Whereas the equatorial scans were sensitive only to the molecular shifts in the $a-b$ plane, modeling of the K scan involves all the parameters related to the structural packing of the molecules. In the rigid molecule approximation, this includes the setting angles (equivalent to displacements along the molecular axis) (4 parameters), molecular handedness (3), and relative positions (6), giving a total of 13 free parameters. Taking the limited amount of data into account, and also the experimental uncertainty, we did not consider it fruitful to attempt a further refinement of these parameters.

Preliminary studies of the other PTFE phases indicated that the thin film phase transition corresponding to the 19 °C bulk II/IV transition is shifted to lower temperatures by at least 10 °C. The 1.3 Å peak splitting shown in Figure 9 demonstrates unambiguously that there is a transition to a low temperature phase. This is important to rule out speculations that the studied thin film phase might somehow be a mixture of the bulk phases II and IV or even that the film phase studied might correspond to the low-temperature bulk phase.

It seems reasonable to assert that the structures of the bar (bulk) and the thin film are sufficiently similar

(see Figure 5) to consider them as respectively low and high ordered versions of the same phase. Figures 1 and 11 illustrate this possibility. If the slight displacements of the molecules get disordered or vanish, i.e., the mean of δ is 0, the unit cell will effectively be single stem as far as equatorial reflections ($l = 0$) are concerned. It seems natural to state that the high degree of biaxial order induced by the substrate (in contrast to the uniaxial order of the bar) is the reason why the fractional order peaks can be observed in the thin film. The high degree of "rotational" orientation (angle χ) about the molecular axis might de facto increase the tendency of alternating packing of right- and left-handed helices, thus promoting the displacements being interpreted as attraction between molecules of opposite handedness. Alternatively, the structure is actually similar in the bar and the thin film, and the high degree of rotational orientation merely facilitates the observation (due to reduced averaging in χ) of the weak fractional order peaks in the thin film case.

Further support for the idea of a gradual transition between a high- and less-ordered structure of phase IV is given by the fact that films produced under slightly different deposition conditions exhibited different degrees of this particular kind of order, for which the intensity ratio of the $1-{}^1/_2 0$ and 100 peaks is a good measure.

Conclusions

Using the friction-transfer technique, PTFE films with the chains being essentially completely aligned in the sliding direction were obtained. TOF-SIMS suggests a coverage of up to 95% of a highly corrugated thin PTFE film. Using GID, we measured a high degree of biaxial orientation for the thin films, parametrized with an in-plane rocking scan peak width of 0.23° and an out-of-plane width ~8°. For the bar used for the friction transfer depositions, a high degree of uniaxial orientation parallel to the deposition direction was found.

The most homogeneous films were obtained using a sliding rate of 0.9 mm/s, applied pressure 0.4 MPa, and temperatures just below the melting point of PTFE. An additional important parameter turned out to be the "deposition history" of the bar. Repeated depositions increased the crystalline order in the bar, yielding films of better quality. Strong indications were found that this crystalline order in the bar relaxed during a period of the order of weeks. With better-ordered bar conditions, the best films were obtained at a lower deposition temperature. The much higher degree of orientation found in the deposited films than in the bars leads to the conclusion that an important part of the friction deposition mechanism is that PTFE strands get attached to the (glass) substrate and are pulled out of the bulk to yield the excellent alignment. Further evidence for this mechanism is given by the fact that entangled and entanglement-free PTFE bars exhibit similar deposition characteristics.

From studies of the thin film structures and detailed structure factor simulations, we conclude that subtle changes of the deposition conditions may cause significant differences in the crystalline order. We have given evidence for the presence of a multistem unit cell, with a four-stem cell appearing as the simplest model to reproduce the experimental data. Further, we have discussed the possibility of a continuous transition between this unit cell and the formerly reported hexagonal single-stem cell. The multistem cell, suggesting alternating left- and right-handed helices, has not previously been reported experimentally for PTFE phase IV.

Acknowledgment. We thank Prof. Paul Smith for many valuable discussions. We are also grateful to Prof. Edward S. Clark and Dr. Natalie Stutzmann for useful suggestions at an early stage of this work. Dansync and the Danish Technical Research Council (STVF) are gratefully acknowledged for financial support.

References and Notes

(1) Bunn, C. W.; Howells, E. R. *Nature (London)* **1954**, *174*, 549.
(2) Pooley, C. M.; Tabor, D. *Proc. R. Soc. London* **1972**, *A329*, 251.
(3) Wittmann, J. C.; Smith, P. *Nature (London)* **1991**, *352*, 414.
(4) Motamedi, F.; Ihn; K. J.; Fenwick, D.; Wittmann, J.-C.; Smith, P. *J. Polym. Sci., Polym. Phys. Ed.* **1994**, *32*, 453.
(5) Bunk, O.; Nielsen, M. M.; Sølling, T. I.; van de Craats, A. M.; Stutzmann, N. *J. Am. Chem. Soc.* **2003**, *125*, 2252.
(6) Miller, R. L. In *Polymer Handbook*, 4th ed.; Brandrup, J., Immergut, E. H., Grulke, E. A., Eds.; Wiley-Interscience: New York, 1999; p VI-159.
(7) Clark, E. S.; Muus, L. T. *Z. Kristallogr.* **1962**, *117*, 119.
(8) Weeks, J. J.; Clark, E. S.; Eby, R. K. *Polymer* **1981**, *22*, 1480.
(9) Clark, E. S. *Polymer* **1999**, *40*, 4659.
(10) Fenwick, D.; Ihn, K. J.; Motamedi, F.; Smith, P.; Wittmann, J. C. *J. Appl. Polym. Sci.* **1993**, *50*, 1151.
(11) Tanigaki, N.; Yoshida, Y.; Kaito, A.; Yase, K. *J. Polym. Sci., Part B: Polym. Phys.* **2001**, *39*, 432.
(12) Hansma, H.; Motamedi, F.; Smith, P.; Hansma, P.; Wittmann, J. C. *Polymer Commun.* **1992**, *33*, 647.
(13) Dietz, P.; Hansma, P. K.; Ihn, K. J.; Motamedi, F.; Smith, P. *J. Mater. Sci.* **1993**, *28*, 1372.
(14) Bodö, P.; Schott, M. *Thin Solid Films* **1996**, *286*, 98.
(15) Flack, H. D. *J. Polym. Sci., Part A2* **1972**, *10*, 1799.
(16) Yamamoto, T.; Hara, T. *Polymer* **1982**, *23*, 521.
(17) Cochran, W.; Crick, F. H. C.; Vand, V. *Acta Crystallogr.* **1952**, *5*, 581.
(18) Clark, E. S.; Weeks, J. J.; Eby, R. K. *ACS Symp. Ser.* **1980**, *141*, 183.
(19) Plummer, C. J. G.; Kausch, H.-H. *Polym. Bull. (Berlin)* **1996**, *37*, 393.
(20) Farmer, B. L.; Eby, R. K. *Polymer* **1985**, *26*, 1944.
(21) Yamamoto, T.; Hara, T. *Polymer* **1986**, *27*, 986.
(22) Holt, D. B.; Farmer, B. L. *Polymer* **1999**, *40*, 4673.
(23) Savin, A. V.; Manevitch, L. I. *Phys. Rev. B* **2001**, *63*, 224303.
(24) Kimmig, M.; Strobl, G.; Stühn, B. *Macromolecules* **1994**, *27*, 2481.
(25) Als-Nielsen, J.; McMorrow, D. *Elements of Modern X-ray Physics,* 1st ed.; John Wiley & Sons: New York, 2001.
(26) Bunk, O.; Nielsen, M. M. *J. Appl. Crystallogr.* **2004**, *37*, 216.
(27) Warren, B. E. *X-ray Diffraction*, 2nd ed.; Dover Publications: New York, 1990; Chapter 13.
(28) Smilgies, D.-M. *Rev. Sci. Instrum.* **2002**, *73*, 1706.
(29) Vickerman, J. C.; Briggs, D. *TOF-SIMS Surface Analysis by Mass Spectrometry*; IM Publications and Surface Spectra Limited, 2001.
(30) Breiby, D. W.; Samuelsen, E. J. *J. Polym. Sci., Polym. Phys. Ed.* **2003**, *41*, 2375.
(31) Smith, P. Private communication.
(32) McLeish, T. C. B.; Plummer, C. J. G.; Donald, A. M. *Polymer* **1989**, *30*, 1651.
(33) deGennes, P. G. *J. Chem. Phys.* **1971**, *55*, 572.

MA0492465